Monte Carlo simulation of the nonequilibrium phase transition in *p*-type Ge at impurity breakdown

W. Quade, G. Hüpper,* and E. Schöll
Institut für Theoretische Physik, Technische Universität Berlin, Hardenbergstrasse 36, 10623 Berlin, Germany

T. Kuhn
Institut für Theoretische Physik, Universität Stuttgart, Pfaffenwaldring 57, 70550 Stuttgart, Germany
(Received 18 November 1993; revised manuscript received 31 January 1994)

We report an ensemble Monte Carlo simulation of impact-ionization-induced impurity breakdown in *p*-type germanium at liquid-helium temperatures. In our Monte Carlo simulation, the impurities are treated as two-level systems (ground state and first excited state) exchanging particles with the continuum of free holes by capture and thermal generation from the excited level and by impact ionization from both levels. From the simulation we directly obtain the experimentally observed negative differential mobility and demonstrate the cooling effect of the impact-ionization process. For a detailed analysis of the nonequilibrium phase transition between low and high conducting states we extract the characteristic relaxation times of fluctuations exhibiting "critical slowing down" and a strong increase of the current-noise spectral density in the phase-transition regime. Finally, we demonstrate that our Monte Carlo simulations can be used for a quantitative investigation of the complex nonlinear dynamics of current filaments in semiconductors.

I. INTRODUCTION

During the last ten years impurity breakdown in semiconductors[1] at liquid-helium temperature has been of large interest both from experimental and theoretical points of view. In the breakdown region, critical and nonlinear dynamic phenomena have been found.[2–7] Up to now theoretical models which describe this nonequilibrium phase transition have been based almost exclusively on approximate solutions of the Boltzmann equation, e.g., on the method of moment equations. They are able to explain qualitatively some of the experimentally observed phenomena, but often fail to give particular details such as, for example, the correct order of magnitude of the measured quantities. On the other hand, these details are closely connected to the microscopic physics involved, and their analysis should allow one to discriminate between different theoretically derived microscopic models. For example, concerning impact ionization, a variety of different theoretical models for the impact-ionization scattering rate[8–10] lead to the same qualitative behavior in the breakdown regime. Indeed, two aspects of impact ionization, namely the fact that it is a process with a threshold and that it is autocatalytic, are mainly decisive for the impurity breakdown. But the quantitative dependence of the impact-ionization rate on the electric field, and its influence on energy and momentum relaxation, are determined by the microscopic model.

It is the purpose of this paper to bridge the gap between the microscopic physics and the macroscopic nonlinear phenomena in the regime of impurity breakdown. In particular, we present a detailed microscopic theory of the scattering processes and generation-recombination (GR) kinetics, which can be used in simulations of the macroscopic spatiotemporal dynamics of current filaments as demonstrated recently in exemplary studies.[11,12]

In previous work,[13] we used a single-particle Monte Carlo simulator to obtain the GR rate coefficients governing the dynamics between the band and impurity levels under nonequilibrium conditions. However, a major restriction of this analysis was that it considered only a single impurity level, and therefore could not explain *S*-shaped negative differential conductivity (SNDC) and the formation of current filaments. To improve the microscopic physics, here we extend this approach with respect to several aspects: First, we now use a many-particle Monte Carlo simulator which allows us to perform direct simulations of time-dependent processes and to overcome some of the restrictive assumptions of the previous single-particle version; second, we treat the impurities as two-level systems, which is a necessary prerequisite for the occurrence of SNDC and current filamentation;[1] and third, the modeling of impact ionization is based on a microscopic model in which, in contrast to previous work[8] and along the lines of Ref. 14, the wave-vector dependence of the matrix element is taken into account. This is important for the asymptotic behavior of the microscopic scattering rate at high energies.

Impurity breakdown in semiconductors leads to an increase of the free-carrier concentration by several orders of magnitude. Such strong particle number variations represent a difficulty for the conventional Monte Carlo simulator.[15] Time-dependent statistical weights for the single electron can be used[16] to overcome the problem of bad statistics in the prebreakdown regime on one hand, and overly free-carrier numbers in the postbreakdown regime on the other hand. Furthermore, strongly different time scales for the scattering processes in the band continuum (10^{-12} s) and for the transition of carriers between the discrete impurity levels (10^{3} s) require a different handling of free and bound carriers.

The paper is organized as follows: The GR model is described in Sec. II. In Sec. III we introduce the Monte Carlo technique and, in particular, explain the choice of

time-dependent statistical weights and the handling of the two bound levels in connection with the continuum of free holes. Section IV presents the direct results of the Monte Carlo simulation. In Sec. V we analyze the dynamics of fluctuations in the phase-transition regime within a master-equation approach, where the transition rates are obtained from the Monte Carlo simulation. Critical slowing down is well reproduced in the relaxation rates of number fluctuations and in the low-frequency noise spectrum. A nonequilibrium phase transition is often accompanied by characteristic features of nonlinear dynamics such as spatial or temporal pattern formation. In Sec. VI we give an example of how Monte Carlo data can be used in the quantitative analysis of the formation and dynamics of current filaments. Finally, in Sec. VII we draw some conclusions. Details concerning the calculation of the thermal generation and recombination rates are given in Appendix A, and the impact ionization rates are derived in Appendix B.

II. THE GENERATION-RECOMBINATION KINETICS

The low-temperature breakdown of doped semiconductors is based on the impact ionization of shallow-impurity states. Therefore, one should expect an important influence of the details of the impurity itself. However, the impurity is normally treated as a simple one-level system with a well-defined energy below the band edge. The infinitely many hydrogenlike discrete states are thought to be lumped into one. In this picture, the time that a carrier remains trapped has the meaning of a mean trapping time only. Within this strongly simplifying approach the occurrence of breakdown can be described; however, details are often in contrast to experiments. Of course, the exact treatment of all impurity states in a Monte Carlo simulator under nonequilibrium conditions is beyond the present possibilities. (Some results concerning the dynamics at thermal equilibrium can be found in Ref. 17.) Nevertheless it can be shown analytically that the impurity must be treated at least as a two-level system in order to describe the experimentally observed S-shaped current-voltage characteristics in the breakdown region.[1] In the following we consider a p-type semiconductor and use the hole picture.

On a macroscopic level, the carrier (hole) concentrations in the three subsystems, i.e., the impurity ground state (p_{t1}), the impurity excited state (p_{t2}), and the valence-band continuum (p) obey the following set of rate equations:[1]

$$\dot{p}=X_1^S p_{t2}-T_1^S p n_t+X_1^* p p_{t2}+X_1 p p_{t1} , \tag{1}$$

$$\dot{p}_{t1}=-X^* p_{t1}+T^* p_{t2}-X_1 p p_{t1} . \tag{2}$$

The concentration p_{t2} is fixed by the charge neutrality condition $p+p_{t1}+p_{t2}=N_A-N_D$, where N_A is the acceptor concentration, $N_D<N_A$ the concentration of compensating donors, and $n_t=N_D+p$ the concentration of ionized acceptors. Equation (1) is a balance of the rate of change of the free-carrier concentration p due to thermal generation from the excited impurity level (coefficient X_1^S), its inverse process (capture coefficient T_1^S), impact ionization from the excited state (coefficient X_1^*) and from the ground state (coefficient X_1). Equation (2) is the balance for the impurity ground state, where the first term (coefficient X^*) describes the thermal excitation of holes into the excited impurity level, the second term (coefficient T^*) the reverse process, and the third term the transition to the band due to impact ionization. In these rate equations the process inverse to impact ionization, i.e., the Auger process, has been neglected. This is justified as long as the impurity concentration is sufficiently low, as is the case in the present studies. For the same reason the carriers in the band are assumed to be nondegenerate.

The problem, of course, is the determination of these coefficients from microscopic transition probabilities under nonequilibrium conditions. Many theoretical predictions about nonlinear phenomena and chaos can be made on the basis of Eqs. (1) and (2), but often the GR coefficients are approximated by phenomenological functions of some control parameter such as, e.g., internal electric field or mean carrier energy.[7] In a more microscopic approach the coefficients depend on the carrier distribution function and therefore can be calculated from a Monte Carlo simulation. On the other hand, by comparing the results of Monte Carlo simulations with experiments, some constants in the microscopic formulas may be determined.

For the Monte Carlo simulation we need the microscopic transition rates between the impurity ground state, the excited state, and the states in the band specified by the wave vector $\mathbf{k}$. Let us first concentrate on the thermal excitation and trapping processes. Neglecting the Poole-Frenkel effect, which describes the influence of the electric field on the impurity states, the coefficients T^*, X^*, and X_1^S are independent of the field. The capture coefficient T_1^S is obtained from the microscopic rate $\mathcal{C}_{\rm rec}(\mathbf{k})$ for the capture of a carrier with wave vector $\mathbf{k}$ by averaging with respect to the distribution function $f(\mathbf{k})$ of the carriers in the band according to

$$T_1^S=\langle \mathcal{C}_{\rm rec}\rangle \equiv \frac{1}{p}\int d^3k\, \mathcal{C}_{\rm rec}(\mathbf{k}) f(\mathbf{k}) , \tag{3}$$

with $p=\int d^3k\, f(\mathbf{k})$. For low temperatures at thermal equilibrium, where impact-ionization processes are negligible, a carrier which is captured by the excited state reaches the ground state with a very large probability. This allows one also to apply the expression for $\mathcal{C}_{\rm rec}$ obtained within the "cascade capture model" (Refs. 10, 18, and 19) (see Appendix A) in the case of a two-level model. The generation rate X_1^S is then determined by detailed balance from the equilibrium coefficient $T_1^{S^0}$ and the thermal equilibrium concentrations p^0, p_{t2}^0, and n_t^0 according to

$$X_1^S=\frac{n_t^0 p^0}{p_{t2}^0} T_1^{S^0} \equiv p_{\rm eff} T_1^{S^0} . \tag{4}$$

The calculation of the equilibrium concentrations from statistical mechanics is given in Appendix A. The transi-

tion probability per unit time of carriers from the excited impurity level to the band state $\mathbf{k}$ is similarly determined by detailed balance as

$$\mathcal{P}_{\text{gen}}(\mathbf{k})=\frac{p_{\text{eff}}}{p^0}\mathcal{C}_{\text{rec}}(\mathbf{k})f^0(\mathbf{k}) , \tag{5}$$

with the equilibrium distribution function $f^0(\mathbf{k})$. The transition coefficients T^* and X^* between the impurity levels are also related by detailed balance:

$$\frac{X^*}{T^*}=\frac{p_{t2}^0}{p_{t1}^0} . \tag{6}$$

Finally, the generation coefficient X^* is fixed by the assumption that, since the slowest step for a carrier to reach the band continuum is to come to the first excited state, the generation coefficient from the ground state to the excited state in the two-level model is approximately equal to the generation coefficient $(X_1^S)^{\text{single}}$ in the one-level model:

$$X^*\approx(X_1^S)^{\text{single}} , \tag{7}$$

which again is related to $T_1^{S^0}$ by detailed balance:

$$(X_1^S)^{\text{single}}=(p_{\text{eff}})^{\text{single}}T_1^{S^0} , \tag{8}$$

where

$$(p_{\text{eff}})^{\text{single}}=N_v(T_L)\exp(E_1/(k_B T_L)) \tag{9}$$

is obtained in analogy with the two-level model (Appendix A).

We are now left with the determination of the two impact-ionization coefficients for the first and the second impurity levels. They are related to the microscopic impact-ionization scattering rate $P_{ii}^{(t)}$ from the impurity level t ($t=t1$ and $t2$) according to

$$X_1=\frac{1}{p}\int d^3k\, P_{ii}^{t1}(\mathbf{k})f(\mathbf{k}) , \tag{10}$$

$$X_1^*=\frac{1}{p}\int d^3k\, P_{ii}^{t2}(\mathbf{k})f(\mathbf{k}) . \tag{11}$$

The microscopic rates are given by

$$P_{ii}^{(t)}(\mathbf{k})=\sum_{\mathbf{k}'}\sum_{\mathbf{k}''}\sum_{\text{impurities}}\frac{2\pi}{\hbar}|M_t|^2\delta[E(\mathbf{k}')+E(\mathbf{k}'')+E_t-E(\mathbf{k})]f_t , \tag{12}$$

with the energy of the impurity level $E_t=(\hbar^2\alpha_t^2)/(2m_v)$, expressed in terms of an effective Bohr radius α_t, the effective mass in the valence band m_v, and the interaction matrix element M_t. Again nondegenerate statistics are assumed, $1-f(\mathbf{k}')\approx 1$ and $1-f(\mathbf{k}'')\approx 1$, and the sums run over all final band states $\mathbf{k}'$ and $\mathbf{k}''$. The occupation probability f_t of state t satisfies

$$\sum_{\text{impurities}} f_t=p_t V \quad (t=t_1,t_2) , \tag{13}$$

where V is the volume of the crystal.

Assuming an impurity wave function similar to the hydrogen ground state, the square of the matrix element is given by

$$|M_t|^2=\left[\frac{e^2}{\epsilon\epsilon_0 V}\right]^2\frac{|F_{vv}|^2|F_{vt}|^2}{(q^2+\lambda^2)^2}\frac{64\pi}{V}\frac{\alpha_t^{5/2}}{(q'^2+\alpha_t^2)^4} , \tag{14}$$

with $\mathbf{q}=-(\mathbf{k}'-\mathbf{k})$ and $\mathbf{q}'=-(\mathbf{k}''+\mathbf{q})$. Here F_{vv} and F_{vt} are overlap integrals between two valence-band states, and between a valence-band state and the impurity state, respectively, ϵ_0 and ϵ are the vacuum and relative static dielectric constants, respectively, and λ is a screening wave vector. Details of the derivation are given in Appendix B.

With the characteristic inverse impact-ionization scattering time

$$\tau_{ii}^{-1}=\frac{1}{\pi}|F_{vv}|^2|F_{vt}|^2\left[\frac{e^2 m_v^{1/2}}{\epsilon\epsilon_0\hbar^{3/2}}\right]^2 , \tag{15}$$

for $k\geq\alpha_t$ we obtain

$$P_{ii}^{(t)}(\mathbf{k})=\tau_{ii}^{-1}\frac{p_t}{3\pi k\alpha_t^2}\int_{q_m}^{q_M}dq\frac{q}{[q^2+(\lambda/\alpha_t)^2]^2}h(q) , \tag{16}$$

with

$$q_M=\frac{k}{\alpha_t}+\sqrt{(k/\alpha_t)^2-1} , \tag{17}$$

$$q_m=\frac{k}{\alpha_t}-\sqrt{(k/\alpha_t)^2-1} , \tag{18}$$

and $P_{ii}^{(t)}(\mathbf{k})=0$ for $k<\alpha_t$. The function $h(q)$ is given in Appendix B. The remaining integration can only be done numerically, and the results for the first and the second impurity levels are shown in Fig. 1.

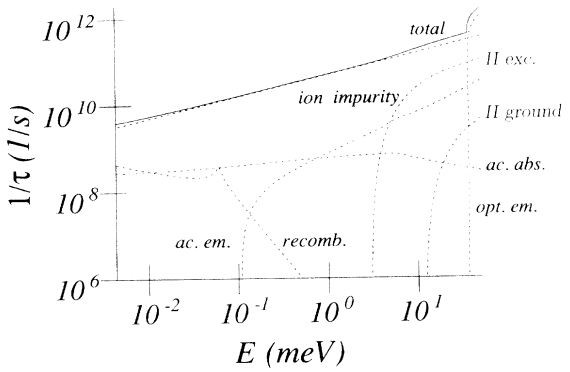

FIG. 1. The microscopic scattering rates as functions of the carrier energy used in the Monte Carlo simulation: acoustic-phonon absorption (ac. abs.) and emission (ac. em.), optical-phonon emission (opt. em.), ionized-impurity (ion. impurity), impact ionization from ground (II ground) and excited (II exc.) state, and capture (recomb.). The rates are calculated for holes in Germanium at a lattice temperature of 4.2 K (see Table I).

III. THE MONTE CARLO TECHNIQUE

We have performed calculations for the case of p-type Ge at 4 K. In this temperature range the relevant scattering processes are elastic scattering from ionized impurities, inelastic acoustic and optical deformation po-

tential scattering, capture by and thermal generation from the excited impurity levels, and impact ionization from both ground and excited impurity levels.[20] The microscopic rates of these scattering processes are shown in Fig. 1. A single band, the heavy-hole band, is taken in the spherical parabolic approximation. In addition to these processes which involve free carriers, our ensemble Monte Carlo simulator accounts for the thermal transitions of the bound carriers between ground and excited impurity levels. It should be emphasized that we distinguish between the *microscopic* scattering and transition rates of the individual carriers (Fig. 1), which are used as input in the Monte Carlo procedure, and the *macroscopic* GR rates, which are obtained as a result of the simulation. The GR coefficients T_1^S, X_1, and X_1^* are calculated from Eqs. (3), (10), and (11) using the distribution function f determined by the Monte Carlo simulation. The GR coefficients X_1^S, X^*, and T^*, however, are (for nondegenerate statistics, and neglecting the Poole-Frenkel effect) independent of the electric field and the distribution function, and can therefore be used as constant input parameters. Their value is determined from detailed balance arguments in thermal equilibrium, as discussed in Sec. II and Appendix A. All parameters of the simulation are summarized in Table I. Further details of a general Monte Carlo simulator can be found in Refs. 15, 21, and 22.

In the following we concentrate on the description of our treatment of the large density variations in the phase-transition regime, and of the very different time scales involved in the problem. To overcome the difficulties introduced by the large free- and bound-carrier density variations, each particle i (which we will call quasiparticle in the following) of $\mathcal{N}_0$ total particles of our simulation represents a time-dependent statistical weight $G_i(t)$ with

$$\sum_{i=1}^{\mathcal{N}_0} G_i(t)=\mathcal{N}_A^*=V(N_A-N_D)\ , \tag{19}$$

where $\mathcal{N}_A^*$ is the effective number of available carriers. With auxiliary functions $\Theta_i(t)$, $\Theta_i^{t1}(t)$, and $\Theta_i^{t2}(t)$, which are equal to 1 if particle i is in the valance band, the impurity ground state, and the excited state, respectively, and equal to zero otherwise, the densities in the three subsystems can be written as

$$p(t)=V^{-1}\sum_{i=1}^{\mathcal{N}_0} G_i(t)\Theta_i(t)\ , \tag{20}$$

$$p_{t1}(t)=V^{-1}\sum_{i=1}^{\mathcal{N}_0} G_i(t)\Theta_i^{t1}(t)\ , \tag{21}$$

$$p_{t2}(t)=V^{-1}\sum_{i=1}^{\mathcal{N}_0} G_i(t)\Theta_i^{t2}(t)\ . \tag{22}$$

The distribution function of the free carriers reads

$$f(\mathbf{k},t)=V^{-1}\sum_{i=1}^{\mathcal{N}_0} G_i(t)\Theta_i(t)\delta[\mathbf{k}-\mathbf{k}_i(t)]\ , \tag{23}$$

where $\hbar\mathbf{k}_i(t)$ is the crystal momentum of particle i at time t. The statistical weight $G_i(t)$ is kept constant until the number of quasiparticles in the valence band $\mathcal{N}_{\text{free}}(t)=\sum_{i=1}^{\mathcal{N}_0}\Theta_i(t)$ falls below $\mathcal{N}_{\min}$ or exceeds $\mathcal{N}_{\max}$ with $0<\mathcal{N}_{\min}<\mathcal{N}_{\max}<\mathcal{N}_0$. In that case the quasiparticles are redistributed according to a statistical method reported in Ref. 16, and thus a new distribution of quasiparticles is generated with unchanged statistical properties.

Besides the large density variations, the second difficulty is the presence of strongly different scattering rates for the relevant scattering processes. Fast intraband processes such as impurity scattering which are mainly responsible for the mobility of the carriers occur on a time scale of 10^{-12} s. In contrast to this, the time scale related to a transition by thermal excitation of a carrier from the ground state to the excited state of the impurities is about 10^3 s. The resulting extreme ratio of the time scales does not permit a direct simulation of all processes. However, since the carriers in each bound state are indistinguishable, we do not need to observe each particle in the bound states individually, but only

TABLE I. Material parameters for p-type Ge at $T_L=4.2$ K used in the simulations (Ref. 15).

Effective mass	$m_v=0.346m_0$
Crystal density	$\rho_0=5.32$ g/cm^3
Sound velocity	$u=3.93\times10^5$ cm/s
Optical-phonon temperature	$\hbar\omega_{\text{op}}/k_B=430$ K
Relativistic static dielectric constant	$\epsilon=16$
Acoustic deformation potential	$E_1^0=4.6$ eV
Optical deformation potential	$d_0/a_0=7.12\times10^8$ eV cm^{-1}
Equilibrium capture coefficient	$T_1^{S0}=6.5\times10^{-5}$ cm^{3}s^{-1}
Excited-state generation coefficient	$X_1^S=1.40\times10^6$ s^{-1}
Ground-state generation coefficient	$X^*=1.00\times10^{-3}$ s^{-1}
Ground-state relaxation coefficient	$T^*=7.21\times10^7$ s^{-1}
Energy of the acceptor ground state	$E_1=12$ meV
Energy of the acceptor excited state	$E_2=3$ meV
Acceptor concentration	$N_A=10^{14}$ cm^{-3}
Donor concentration	$N_D=10^{12}$ cm^{-3}

their total statistical weights:

$$G_{t1}(t)=\sum_{i=1}^{\mathcal{N}_0} G_i(t)\Theta_i^{t1}(t)\ , \tag{24}$$

$$G_{t2}(t)=\sum_{i=1}^{\mathcal{N}_0} G_i(t)\Theta_i^{t2}(t)\ . \tag{25}$$

Thus, if we are interested only in mean values, we can neglect the statistical fluctuations of the carrier densities and take care of the most critical processes (transitions between the bound states) in terms of rate equations without loss of microscopic information. For the Monte Carlo simulation this means that the particles do not make transitions between the bound states (due to thermal excitation and relaxation), but their total statistical weights change continuously according to the rate equations[1]

$$\left[\frac{d}{dt}\right]' G_{t1}=+T^* G_{t2}-X^* G_{t1}\ , \tag{26}$$

$$\left[\frac{d}{dt}\right]' G_{t2}=-T^* G_{t2}+X^* G_{t1}\ . \tag{27}$$

The prime at the time derivative indicates that these rate equations describe only the influence of the exchange of particles between the bound states. The additional change of the statistical weights due to impact-ionization processes and other band-impurity transitions is then obtained from the Monte Carlo simulation.

IV. SIMULATION RESULTS

In the breakdown regime a Monte Carlo simulation faces serious problems, some of which have already been mentioned in the previous sections. When using a two-level model for the impurities, additional difficulties arise due to the fact that then the carrier-density-voltage characteristic may in principle be S shaped,[1] depending on the degree of the compensation. In this case, for certain fixed values of the electric field, there exist unstable stationary states as well as possibly oscillatory instabilities induced by fluctuations. Since the Monte Carlo simulator represents the physical system including noise, all these features may occur in the simulations. In order to obtain a stable static characteristic for the mean values, we have chosen a compensation N_D sufficiently small (see Table I) such that no S shape occurred.

The steady-state values for mean energy E, mean velocity v, and carrier densities of the three subsystems p, p_{t1}, and p_{t2} are shown in Fig. 2 as functions of the electric field $\mathcal{E}$. The threshold behavior of the free-carrier density p at $\mathcal{E}=1.8$ V/cm is clearly seen, reflecting the nonequilibrium phase transition from a low- to a high-conductivity state. In contrast to the monotonic increase of p, the carrier density in the excited impurity level p_{t2} first also increases sharply, but then, for higher fields, decreases again. The reason is that at very low fields all carriers are found in the ground state of the impurities; consequently p and p_{t2} are small. Then, with increasing field, impact ionization from the ground state sets in, p rises and, due

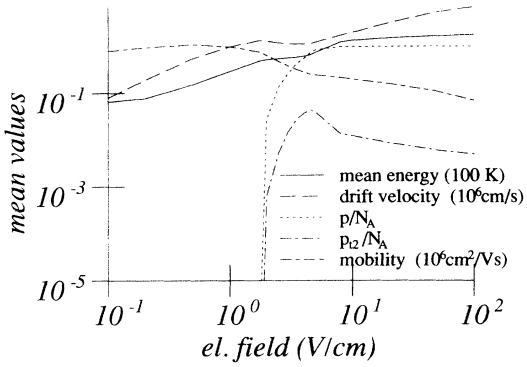

FIG. 2. Mean values of the carrier energy E (expressed in units of 100 K in terms of a carrier temperature $k_B T_h = E$), the drift velocity v in units of 10^6 cm/s, the free-carrier concentration p/N_A, the concentration p_{t2}/N_A of the excited impurity level, and the mobility in units of 10^6 cm^2/V s as functions of the electric field.

to thermal recombination, so does p_{t2}. Finally, the density in the excited level decreases due to stronger impact ionization. For the drift velocity v we first obtain, in the prebreakdown regime, an almost linear increase with respect to the field and then, immediately after the strong rise in the carrier concentration p, a range of negative differential mobility $dv/d\mathcal{E}$. The reason is the enhanced ionized impurity scattering in that regime, which leads to a decrease in the momentum relaxation time. On the other hand, the plateau in the field dependence of the mean energy in the same field region just above threshold is due to the efficient cooling by impact-ionization processes. The phenomenon that in the breakdown regime the mean energy remains constant and the mean velocity even decreases as a function of field, is not at all obvious. It is an elaborate result of our detailed microscopic simulation. It was not obtained in our previous Monte Carlo simulation with a *single* impurity level,[13] but has indeed been found experimentally for low compensation.[4,6] We stress that it is characteristic of the impact-ionization-induced impurity breakdown.

The coefficients X_1, X_1^*, and T_1^S (obtained from the Monte Carlo simulation) multiplied by the acceptor concentration N_A are shown in Fig. 3 together with the inverse momentum (τ_m^{-1}) and energy (τ_e^{-1}) relaxation times as functions of the electric field $\mathcal{E}$. The impact-ionization rates strongly increase with increasing field due to the heating of the carriers. The capture coefficient T_1^S generally decreases with increasing field because less carriers are in the region with small energies from where they can recombine with high probability (see Fig. 1). The pronounced local maximum at about 4 V/cm again is a consequence of impact ionization. In this field range, due to strong impact ionization, many carriers are scattered back to the band minimum. The generated carriers, as well, are placed near that minimum, enhancing the occupation probability at low energies and consequently the recombination probability.

It is interesting to follow the time evolution of the model system from an initial value to its stationary state in the region close to breakdown (Figs. 4 and 5). Due to

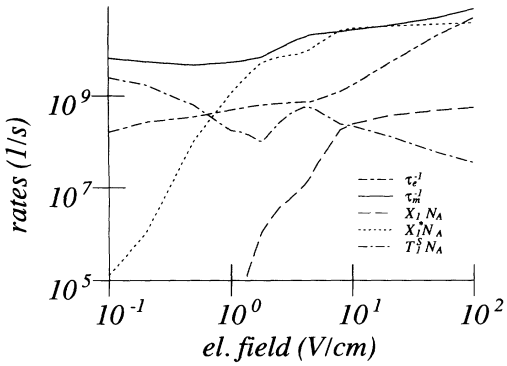

FIG. 3. Inverse momentum (τ_m^{-1}) and energy (τ_E^{-1}) relaxation times, and impact-ionization coefficients from the ground level (X_1) and the excited level (X_1^*), and capture coefficient (T_1^S) as functions of the electric field.

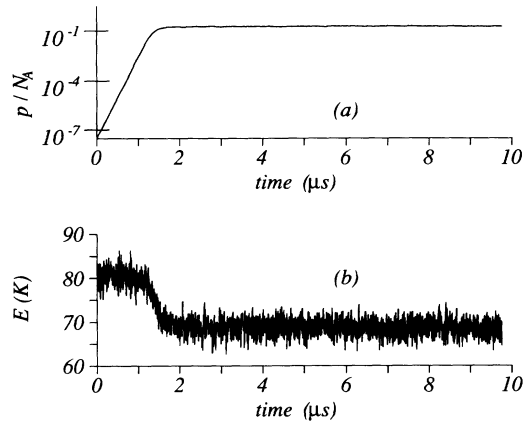

FIG. 5. (a) Free carrier concentration p and (b) mean energy E (in units of T_h with $E=k_B T_h$) as a function of time for an electric field in the postbreakdown regime (3 V/cm).

the critical slowing down of characteristic relaxation times in this regime, which will be discussed in Sec. V, very long times for the relaxation of the system into the steady state can be expected at breakdown ($\mathcal{E}=1.8$ V/cm). This is clearly seen in Fig. 4(b), where the system needs about 25 μs to reach the steady-state carrier concentration. Relaxation to the steady state occurs at least one order of magnitude faster in Fig. 5(a), where the system is well above threshold. In Fig. 5(b) the corresponding mean energy behavior is shown. In the transient regime most carriers are still in the ground state of the impurity. Impact ionization is weak, and does not yet have much influence on the mean energy. The generated carriers recombine into the excited state of the impurity, which becomes more and more occupied. In the stationary state there is mainly a balance between thermal recombination and impact ionization from the excited state. The cooling due to the latter process leads to the reduction of about 10% of the mean energy compared to its initial transient value.

V. NOISE ANALYSIS

The relaxation from an initial state to the stationary state shown in Figs. 4 and 5 gives direct evidence that the characteristic time scales close to breakdown are slowed down strongly. This "critical slowing down" (Ref. 1) can be analyzed more quantitatively by looking at fluctuations from the steady state. Therefore, in this section we present an analysis of the noise properties of the system. We use the technique explained in Ref. 13, here applied to the case of two bound states at the impurities. The current correlation function, which describes the electrical noise of the system, is decomposed into two parts; the contribution due to velocity fluctuations and the contribution due to fluctuations in the number of carriers in the band according to

$$\langle \delta I(0)\delta I(t)\rangle = \frac{e^2}{L^2}[\langle \mathcal{N}\rangle^2\langle \delta v(0)\delta v(t)\rangle + \langle v\rangle^2\langle \delta\mathcal{N}(0)\delta\mathcal{N}(t)\rangle], \tag{28}$$

where $\mathcal{N}(t)$ denotes the number of carriers in the band, $v(t)$ their drift velocity, L the length of the system, and $\delta x(t)=x(t)-\langle x\rangle$ is the actual deviation of a quantity x from its mean value. The velocity contribution is mainly governed by scattering processes inside the band; transitions between the ground state and the band play only a minor role. Its field dependence in the present two-level case practically coincides with the one-level model discussed in detail in Ref. 13. Therefore, here we will concentrate on the second contribution.

The calculations of the number fluctuations are based on the master-equation approach,[23] with transition coefficients obtained from the Monte Carlo simulations. The state of the system is characterized by the number of carriers in the acceptor ground state $\mathcal{N}_{t1}$ and the band $\mathcal{N}$. The number in the excited state $\mathcal{N}_{t2}$ is fixed by particle conservation, $\mathcal{N}_{t1}+\mathcal{N}_{t2}+\mathcal{N}=(N_A-N_D)V$. In order to calculate the number contribution to the current noise, we need the equations of motion for the correlation functions. They are obtained from the rate equations [Eqs. (1) and (2)] by linearization:

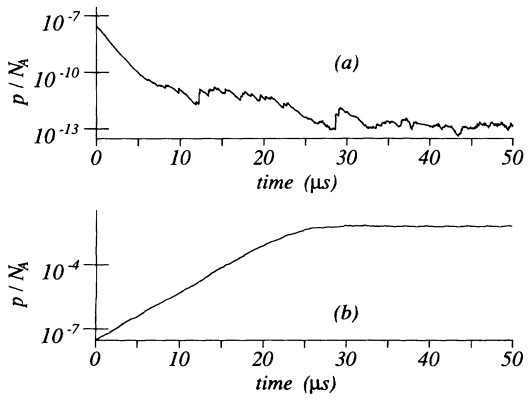

FIG. 4. Free-carrier concentration p as a function of time for an electric field (a) in the prebreakdown regime (1.3 V/cm) and (b) at breakdown (1.8 V/cm). The simulations start with an arbitrarily chosen initial concentration of $p/N_A^*=3\times10^{-8}$.

$$\frac{d}{dt}\langle \delta\mathcal{N}(0)\delta\mathcal{N}(t)\rangle = -a_{11}\langle \delta\mathcal{N}(0)\delta\mathcal{N}(t)\rangle - a_{12}\langle \delta\mathcal{N}(0)\delta\mathcal{N}_{t1}(t)\rangle \ , \quad (29)$$

$$\frac{d}{dt}\langle \delta\mathcal{N}(0)\delta\mathcal{N}_{t1}(t)\rangle = -a_{21}\langle \delta\mathcal{N}(0)\delta\mathcal{N}(t)\rangle - a_{22}\langle \delta\mathcal{N}(0)\delta\mathcal{N}_{t1}(t)\rangle \ , \quad (30)$$

with

$$a_{11} = X_1^S + T_1^S(n_t + p) - X_1^*(p_{t2} - p) - X_1 p_{t1} \ , \quad (31)$$

$$a_{12} = X_1^S + (X_1^* - X_1)p \ , \quad (32)$$

$$a_{21} = T^* + X_1 p_{t1} \ , \quad (33)$$

$$a_{22} = T^* + X^* + X_1 p \ . \quad (34)$$

The time evolution of the two correlation functions is therefore governed by two relaxation times τ_1 and τ_2, the eigenvalues of the matrix a_{ij}, and the autocorrelation function of number fluctuations is given by

$$\langle \delta\mathcal{N}(0)\delta\mathcal{N}(t)\rangle = (c_1\langle \delta\mathcal{N}^2\rangle + c_2\langle \delta\mathcal{N}\delta\mathcal{N}_{t1}\rangle)\exp\left[-\frac{t}{\tau_1}\right] + [(1-c_1)\langle \delta\mathcal{N}^2\rangle - c_2\langle \delta\mathcal{N}\delta\mathcal{N}_{t1}\rangle]\exp\left[-\frac{t}{\tau_2}\right] \quad (35)$$

with the expansion coefficients $c_1 = (a_{11} - \tau_2^{-1})/(\tau_1^{-1} - \tau_2^{-1})$ and $c_2 = a_{12}/(\tau_1^{-1} - \tau_2^{-1})$. In contrast to the case of the one-level model,[13] here the decay of number fluctuations occurs on two time scales. In order to determine the initial values of the correlation functions, the variances are needed. From the master-equation approach the equations of motion for the variances are obtained according to

$$\frac{d}{dt}\langle \delta\mathcal{N}^2\rangle = b_1 - 2a_{11}\langle \delta\mathcal{N}^2\rangle - 2a_{12}\langle \delta\mathcal{N}\delta\mathcal{N}_{t1}\rangle \ , \quad (36)$$

$$\frac{d}{dt}\langle \delta\mathcal{N}\delta\mathcal{N}_{t1}\rangle = b_2 - a_{21}\langle \delta\mathcal{N}^2\rangle - (a_{11} + a_{22})\langle \delta\mathcal{N}\delta\mathcal{N}_{t1}\rangle - a_{12}\langle \delta\mathcal{N}_{t1}^2\rangle \ , \quad (37)$$

$$\frac{d}{dt}\langle \delta\mathcal{N}_{t1}^2\rangle = b_3 - 2a_{21}\langle \delta\mathcal{N}\delta\mathcal{N}_{t1}\rangle - 2a_{22}\langle \delta\mathcal{N}_{t1}^2\rangle \ , \quad (38)$$

with

$$b_1 = V(X_1^S p_{t2} + X_1^* p p_{t2} + T_1^S p n_t + X_1 p p_{t1}) \ , \quad (39)$$

$$b_2 = -V(X_1 p p_{t1}) \ , \quad (40)$$

$$b_3 = V(T^* p_{t2} + X^* p_{t1} + X_1 p p_{t1}) \ . \quad (41)$$

The variances then can be calculated as steady-state solutions of Eqs. (36)–(38).

The noise current spectral density S_I as a function of frequency f is obtained from the current correlation function according to the Wiener-Khintchine theorem by Fourier transformation.[13] It can be decomposed into a velocity contribution $s_v(f)$ and two number contributions $s_{\mathcal{N}1}$ and $s_{\mathcal{N}2}$ corresponding to the relaxation times τ_1 and τ_2 according to

$$S_I(f) = \frac{4pe^2V}{L^2}s(f) = \frac{4pe^2V}{L^2}[s_v(f) + s_{\mathcal{N}1}(f) + s_{\mathcal{N}2}(f)] \ , \quad (42)$$

with

$$s_{\mathcal{N}1}(f) = [c_1\langle \delta\mathcal{N}^2\rangle + c_2\langle \delta\mathcal{N}\delta\mathcal{N}_{t1}\rangle]\frac{\tau_1}{1+(2\pi f\tau_1)^2} \ , \quad (43)$$

$$s_{\mathcal{N}2}(f) = [(1-c_1)\langle \delta\mathcal{N}^2\rangle - c_2\langle \delta\mathcal{N}\delta\mathcal{N}_{t1}\rangle]\frac{\tau_2}{1+(2\pi f\tau_2)^2} \ . \quad (44)$$

In Fig. 6 the characteristic relaxation rates τ_1^{-1} and τ_2^{-1} are plotted as functions of the electric field. For comparison, the dotted lines show recombination and impact-ionization rates. At fields below 1 V/cm, τ_1 agrees perfectly with the recombination rate $T_1^S N_D$ from the band to the excited level of the impurity (below the breakdown, the concentration of ionized acceptors is equal to N_D), and τ_2 agrees with the rate from the excited to the ground state of the impurity. All generation rates, thermal as well as impact ionization, are much smaller and therefore do not influence the relaxation of number fluctuations. Well above the breakdown, on the other hand, the dominant processes for this relaxation are impact ionization from the ground state and from the excited states. The relaxation rates agree with the impact-ionization rates of carriers in these two states. (The concentration of carriers in the band which can perform impact ionization is approximately $N_A - N_D$.) In the breakdown region, in general the rates are influenced by all processes and, in particular, τ_1^{-1} becomes very small at the phase transition. Due to this critical slowing down, the fluctuations at this point decay more than two orders of magnitude

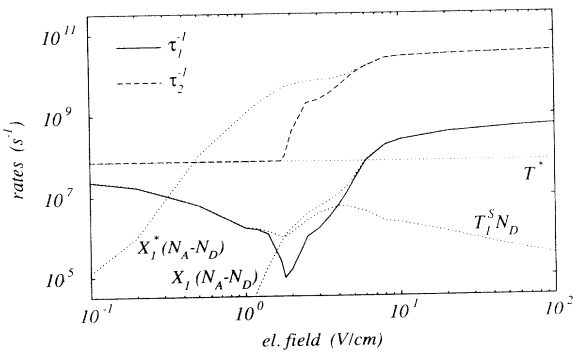

FIG. 6. Characteristic relaxation rates τ_1^{-1} and τ_2^{-1} for carrier number fluctuations as a function of the electric field. Close to the phase transition τ_1^{-1} exhibits a pronounced "critical slowing down." For comparison, capture and impact-ionization rates are included as dotted lines, which make it evident that below the breakdown the relaxation rates are determined by trapping processes, and above the breakdown by impact-ionization processes.

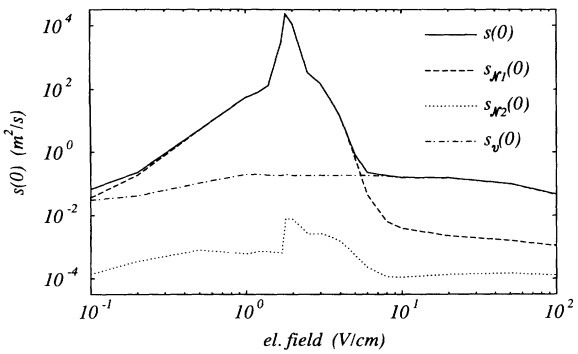

FIG. 7. Contributions to the low-frequency value of the noise spectral density as a function of the electric field. Close to the phase transition the contribution due to number fluctuations associated with the relaxation time τ_1 increases by several orders of magnitude and then strongly decreases with increasing field due to the almost complete ionization of impurities. The contribution associated with τ_2 is always negligible.

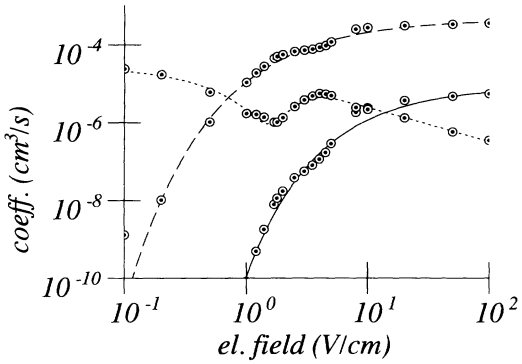

FIG. 8. GR coefficients obtained from the Monte Carlo simulation together with the analytical fit functions $X_1(\mathcal{E})$ (full line), $X_1^*(\mathcal{E})$ (dashed line), and $T_1^S(\mathcal{E})$ (dotted line) used in the analysis of the nonlinear spatiotemporal dynamics.

slower than at low fields, and more than three orders of magnitude slower than at high fields.

In Fig. 7 the three contributions $s_v(0)$, $s_{\mathcal{N}1}(0)$ and $s_{\mathcal{N}2}(0)$ as well as the total value of the low-frequency noise spectral density $s(0)$ are shown as functions of the electric field. The velocity contribution has been taken from the single-particle simulations in Ref. 13. We note again the strong increase in noise at the phase transition by more than four orders of magnitude,[2] which is partly due to the increase of τ_1 and partly due to an increase in the variances. We further note that the contribution with relaxation time τ_2 is always very small and therefore will not be visible in the spectrum. When comparing the results obtained here within the two-level model with the corresponding results obtained within the one-level model (Fig. 6 in Ref. 13), we find that in the present case the number contribution falls below the velocity contribution at much lower fields. The reason is that the ionization of the impurities above breakdown is much more efficient in the two-level case. The carriers which are trapped in the excited state have a very high probability of being excited back into the band due to the high impact ionization rate from this level, and only a small probability to relax into the ground state in which the impact ionization is two orders of magnitude less efficient (see Fig. 1). This strong generation rate is missing in the one-level model.

VI. NONLINEAR DYNAMICS

In this section we present an example of how transport coefficients obtained by our Monte Carlo simulation can be used for a quantitative analysis of the nonlinear spatiotemporal dynamics often associated with the nonequilibrium phase transition at impurity breakdown.[1] In particular, we study the formation and dynamics of current filaments, i.e., self-organized spatiotemporal structures characterized by a current flow which is inhomogeneously distributed in the direction transverse to the electric field. For the numerical analysis the field dependences of the GR coefficients obtained from the Monte Carlo data have been fitted by smooth analytical functions as shown in Fig. 8, and then inserted into the macroscopic semiconductor transport equations.[7,11,12] Increasing the concentration of compensating donors to 5×10^{12} cm^{-3}, the system of equations (1) and (2) yields an S-shaped carrier density versus electric-field characteristics [see Fig. 9(a)]. This leads to an S-shaped current-voltage characteristic [Fig. 9(b)] with a negative differential conductivity branch. The inset of Fig. 9(b) shows a measured characteristic[24] revealing very good agreement with our calculations. For comparison, the characteristic previously calculated from a simple rate equation model with a single acceptor level and phenomenological capture and impact-ionization rates[25] is plotted in Fig. 9(c), exhibiting no negative differential conductivity. It should be noted that S-shaped negative differential conductivity in the two-level model [Fig. 9(b)] arises only if the compensation N_D/N_A exceeds a minimum value, and it becomes the more pronounced the higher the compensation is.[1] Under such conditions, complex and often chaotic temporal behaviors of the current or voltage are possible. While spatially homogeneous conditions are sufficient to explain the physical origin of oscillatory instabilities under the simultaneous action of crossed electric and magnetic fields by the dynamic Hall effect,[25] the investigation of moving filaments which have also been experimentally observed under those conditions[5,6] requires an extension of rate equations (1) and (2) to the spatially inhomogeneous case. In Ref. 12 a semiconductor model has been presented which extends the dynamic Hall effect to filamentary conduction. In that model, traveling and breathing filaments can be obtained. Figure 10 shows density plots of the carrier concentration $n(z,t)$ for different values of the magnetic field. The sample is $W=60$ μm wide and has triangular contacts (which may also serve as a model for nonideal *planar* contacts) spaced $L_0=180$ μm at the center and $L_0+L'=246$ μm at the borders. The magnetic field is applied perpendicular to this plane. The applied current density j_0 is chosen in the regime of negative differential conductivity [Fig. 9(b)]. For small magnetic fields the filament remains near the center of the sample, and shows

asymmetrically breathing filament boundaries [Fig. 10(a)]. For increasing magnetic fields the breathing transforms into regular transverse motion in the direction of the Lorentz force, some way toward the borders of the device where the filament is destroyed. Small regular current oscillations arise due to the periodic nascence and destruction of traveling filaments [Fig. 10(b)]. This motion becomes irregular and chaotic by a further increase of the magnetic field [Fig. 10(c)]. Finally, at still higher magnetic fields, the filament is pinned at the boundary after some transient traveling sequences [Fig. 10(d)]. Such complex behavior agrees well with recent experiments on p-Ge at impurity breakdown.[26] The Monte Carlo data of Fig. 8 have been used in further simulations of the complex spatiotemporal dynamics of current filaments with[12,20] and without[11,20] magnetic fields.

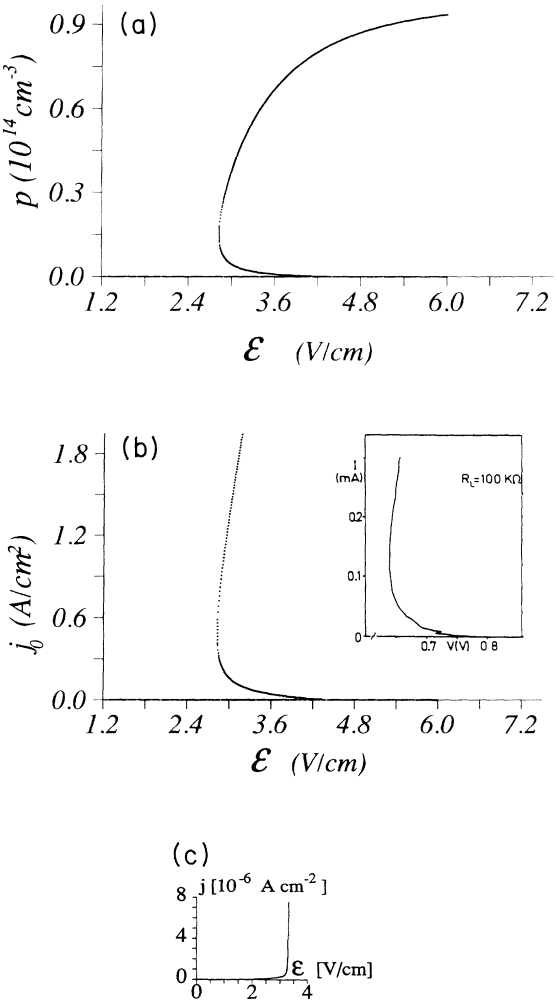

FIG. 9. (a) Carrier density p and (b) current density j_0 as functions of the electric field $\mathcal{E}$ obtained from Eqs. (1) and (2) using the coefficients from the Monte Carlo simulation (Fig. 8) and an enhanced compensation of $N_D=5\times10^{12}$ cm^{-3}. In (b) the inset shows a current-voltage characteristic measured in p-Ge at 4.18 K with a 100-kΩ load resistance (Ref. 24). (c) The current density as a function of the electric field calculated from a phenomenological one-level model (after Ref. 25).

VII. CONCLUSIONS

We have presented a detailed microscopic analysis of the low-temperature breakdown of p-type Ge based on impact ionization from shallow acceptors. The impurities have been treated within a two-level model. We have derived an expression for the impact-ionization rates from both levels which includes the wave-vector dependence and thus exhibits the correct asymptotic energy dependence. These microscopic rates, as well as phonon and impurity scattering and the thermal excitation and trapping rates, then have been used as input for ensemble Monte Carlo simulations of the carrier dynamics. Time-dependent statistical weights have been introduced to overcome the difficulties associated with the strong variations in the carrier concentrations before and after the breakdown, and with the largely different time scales of scattering and thermal generation processes. From simulations we have obtained the mean values of velocity, energy, and carrier concentrations in the various levels, as well as the energy and momentum relaxation times, and the generation-recombination coefficients. A distinct effect of cooling and of negative differential mobility due to impact ionization has been found. An analysis of the

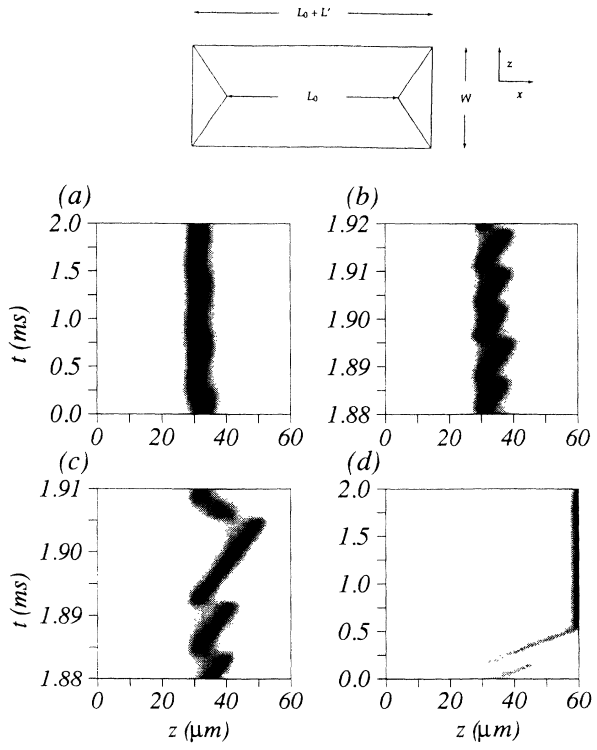

FIG. 10. Density plots of the carrier concentration p as a function of the coordinate z transverse to the electric field, and of time t for different values of the magnetic field. The gray intensity is proportional to the carrier density. (a) $\mathcal{B}=11$ mT, (b) $\mathcal{B}=15$ mT, (c) $\mathcal{B}=20$ mT, and (d) $\mathcal{B}=25$ mT. Numerical parameters as in Fig. 9 with $j_0=0.85$ mA/cm^2. For simplicity a constant mobility $\mu=10^5$ cm^2/V s has been used, which is smaller than in Fig. 2 because of increased N_D. The inset shows the sample configuration with triangular contacts.

time evolution from an initial state to the steady-state solution directly revealed the slowing down of relaxation times at the nonequilibrium phase transition. This critical slowing down, accompanied by a strong increase in the noise power spectrum, was analyzed quantitatively by investigating the dynamics of fluctuations within master-equation formalism. Finally, we have used the GR coefficients obtained from the Monte Carlo simulations for a quantitative analysis of the formation and dynamics of current filaments in the presence of a transverse magnetic field.

The main differences between this model and previous work which used rate equations with simple phenomenological GR coefficients[1,25] is that, in addition to improved impact ionization rates and electron heating effects we can provide a detailed account of the complicated nonmonotonic dependence of the capture rate (Fig. 3) and the mobility (Fig. 2) upon the electric field in the breakdown regime, which has indeed been found experimentally.[6] This is due to the elaborate microscopic physics contained in the various scattering and GR processes, and their mutual nonlinear interactions. With respect to our previous single-particle Monte Carlo simulations using a one-level model,[13] the main improvements are the following. First, the two-level model can reproduce S-shaped negative differential conductivity and current filamentation, including their rich complex nonlinear dynamics. Second, a plateau in the field dependence of the mean energy due to impact-ionization cooling, and a decrease in the drift velocity due to enhanced ionized-impurity scattering, occur in the impurity breakdown regime. Third, the temporal development of the carrier density and its critical slowing down near the nonequilibrium phase transition can be directly followed in our ensemble Monte Carlo (MC) simulations. Limitations of our model include the neglect of higher excited states of the acceptors, the Poole-Frenkel effect, and effects of degenerate statistics or dynamical screening. However, in the regime considered these approximations appear to be appropriate. A further improvement of our model can be obtained by determining the GR coefficients also in the regime of negative differential conductivity directly from a MC simulation.[27]

ACKNOWLEDGMENTS

Two of us (T.K. and W.Q.) acknowledge financial support of the Deutsche Forschungsgemeinschaft (Bonn, Germany). Valuable discussions with K. Pyragas, L. Varani, and L. Reggiani are gratefully acknowledged.

APPENDIX A: THERMAL GENERATION AND RECOMBINATION

Here we will give some details concerning the generation and recombination coefficients T_1^S, X_1^S, T^*, and X^* for the case of an impurity with two discrete levels. The "cascade capture model" (Refs. 18 and 19) gives the probability per unit time at which a free carrier with energy E is captured into the ground state of an attractive impurity:

$$\mathcal{P}_{\rm rec}(E)=n_t\mathcal{C}_{\rm rec}(E)\ , \tag{A1}$$

where n_t is the density of attractive impurities, i.e., ionized acceptors. The microscopic capture coefficient $\mathcal{C}_{\rm rec}(E)$ in the cascade capture model is given by[10]

$$\mathcal{C}_{\rm rec}(E)=\frac{\hbar k}{m_v}\frac{\sigma_1}{x}H(x)\ , \tag{A2}$$

with $x=2E/(m_v u^2)$, $\gamma=2k_B T_L/(m_v u^2)$, $\eta=2|E'|/(m_v u^2)$,

$$H(x)=\int_0^\infty \frac{(x+\eta)^2[1-(1+\eta/\gamma)\exp(-\eta/\gamma)]}{\{[1+(x+\eta)/4)]^2-x\}^3\{1-\exp[-(x+\eta)/\gamma]\}}d\eta\ , \tag{A3}$$

and the cross section

$$\sigma_1=\frac{1}{3}\left[\frac{e^2}{4\pi\epsilon\epsilon_0}\right]^3\frac{(E_1^0)^2}{\rho_0 u^6\hbar^4}\ . \tag{A4}$$

Here m_v is the effective mass, T_L the lattice temperature, E_1^0 the acoustic deformation potential, ρ_0 the crystal density, and u the longitudinal sound velocity. Using this rate, the equilibrium recombination coefficient $T_1^{S^0}$ can be calculated according to Eq. (3) by taking $f(\mathbf{k})$ as the equilibrium distribution function.

For the calculation of the generation rate X_1^S according to Eq. (4), we need the equilibrium concentrations p^0, p_{t2}^0, and n_t^0. Therefore, we calculate the grand-canonical partition function Ξ for the case of a two-level impurity, which can be occupied by $r=0$ or 1 carriers in the energy levels E_l, $l=1$ and 2. Assuming the degeneracy to be g_{rl} ($g_{11}=2$ due to spin for the s-like ground state and $g_{12}=6$ for the p-like excited state) the grand partition function is given by

$$\Xi=\sum_{r=0}^{1}Z_r\lambda^r\ , \tag{A5}$$

where

$$\lambda=\exp(E_F/k_B T_L)\ ,$$

$$Z_0=1\ ,$$

$$Z_1=\textstyle\sum_{l=1}^{2}g_{1l}\exp(-E_l/k_B T_L)\ ,$$

and E_F is the Fermi energy. The probability $p(1,l)$ of finding state l occupied is given by

$$p(1,l)=\Xi^{-1}g_{1l}\lambda\exp\left[\frac{-E_l}{k_B T_L}\right]\ . \tag{A6}$$

The equilibrium density of acceptors with state l occu-

pied (by holes) is obtained by multiplying the probability $p(1,l)$ by the acceptor concentration N_A:

$$p_{t1}^0 = N_A \Xi^{-1} 2 \exp\left[\frac{E_F - E_1}{k_B T_L}\right], \tag{A7}$$

$$p_{t2}^0 = N_A \Xi^{-1} 6 \exp\left[\frac{E_F - E_2}{k_B T_L}\right], \tag{A8}$$

and consequently the densities of occupied ($p_t^0 = p_{t1}^0 + p_{t2}^0$) and vacant ($n_t^0 = N_A - p_t^0$) acceptors are given by

$$p_t^0 = N_A \left[1 + \exp\left[\frac{-E_F + E^*}{k_B T_L}\right]\right]^{-1}, \tag{A9}$$

$$n_t^0 = p_t^0 \exp\left[\frac{-E_F + E^*}{k_B T_L}\right], \tag{A10}$$

where

$$E^* = -k_B T_L \ln\left[2 \exp\left[\frac{-E_1}{k_B T_L}\right] + 6 \exp\left[\frac{-E_2}{k_B T_L}\right]\right]. \tag{A11}$$

The equilibrium carrier density in the valence band is given by

$$p^0 = N_v(T_L) \exp\left[\frac{E_F}{k_B T_L}\right], \tag{A12}$$

with the effective density of states

$$N_v(T_L) = \frac{2(2\pi m_v k_B T_L)^{3/2}}{(2\pi\hbar)^3}, \tag{A13}$$

and the Fermi energy is then fixed by charge conservation $p^0 + p_t^0 = N_A - N_D$. Thus for p_{eff} in Eq. (4) we obtain

$$p_{\text{eff}} = \left[1 + \tfrac{1}{3} \exp\left[\frac{E_2 - E_1}{k_B T_L}\right]\right] N_v(T_L) \exp\left[\frac{E^*}{k_B T_L}\right], \tag{A14}$$

and X_1^S can be calculated.

Finally we need to know the coefficients T^* and X^* which determine the transition rates between ground and excited impurity levels. Their ratio is given by (6) with

$$\frac{p_{t2}^0}{p_{t1}^0} = 3 \exp\left[\frac{E_1 - E_2}{k_B T_L}\right] \tag{A15}$$

following from Eqs. (A7) and (A8).

APPENDIX B: THE IMPACT-IONIZATION MODEL

Following the ideas of Robbins and Landsberg[9] we present here a model for impact ionization from impurities. In contrast to their analytical models, as well as to the widely used Keldysh model,[10] (but similar to Ref. 28), we account for the wave-vector dependence of the matrix element for the electron-electron interaction. The matrix element for impurity impact ionization is

$$M_t = \int d^3x \int d^2y \, \psi_v^*(\mathbf{k}'', \mathbf{x}) \psi_v^*(\mathbf{k}', \mathbf{y}) \times V(\mathbf{x}, \mathbf{y}) \psi_v(\mathbf{k}, \mathbf{y}) \psi_t(\mathbf{x}), \tag{B1}$$

describing the transition of a carrier out of state $\mathbf{k}$ into state $\mathbf{k}'$ by simultaneously exciting the bound carrier ψ_t into the band state $\mathbf{k}''$. The interaction occurs via the screened Coulomb potential

$$V(\mathbf{x}, \mathbf{y}) = \frac{1}{4\pi\epsilon\epsilon_0} \frac{e^2}{|\mathbf{x} - \mathbf{y}|} \exp[-\lambda |\mathbf{x} - \mathbf{y}|]. \tag{B2}$$

For the calculation we assume a spherical parabolic semiconductor and use Bloch waves for the states $\mathbf{k}$, $\mathbf{k}'$, and $\mathbf{k}''$. The bound state ψ_t, which is in principle orthogonal to all band states, is approximated within the envelope function approach by a hydrogenlike function according to

$$\psi_t(\mathbf{x}) \approx u_t(\mathbf{x}) \frac{1}{\sqrt{\pi}} \alpha_t^{3/2} \exp\{-\alpha_t |\mathbf{x}|\}, \tag{B3}$$

where u_t is a function with the periodicity of the lattice. The coefficient $\alpha_t = \sqrt{2 m_c |E_t|}/\hbar$ is an inverse effective Bohr radius of the bound state, and E_t is the binding energy of the impurity level. With these functions the matrix element can be calculated analytically and the result for $|M_t|^2$ is given in Eq. (14).

The impact-ionization rate is then calculated according to Eq. (12), leading to Eq. (16), where the function

$$h(q) = \frac{B}{C^4 - 4q^2 B^2} \times \left\{2 \frac{C^4 + 4q^2 B^2 - 4C^2(q^2+1)}{C^4 - 4q^2 B^2} + 3C^2\right\} + \tfrac{3}{2}\{\arctan(B - q) + \arctan(B + q)\}, \tag{B4}$$

with $B = [(q_M - q)(q - q_m)]^{1/2}$ and $C = [B^2 + q^2 + 1]^{1/2}$ has been introduced.

*Present address: Aescudata GmbH, Bahnhofstr. 56, 21423 Winsen (Luhe), Germany.

[1] E. Schöll, *Nonequilibrium Phase Transitions in Semiconductors* (Springer, Berlin, 1987).
[2] M. Pilkuhn, Z. Naturforsch. **16a**, 173 (1961); **16a**, 182 (1961).
[3] K. Aoki, T. Kobayashi, and K. Yamamoto, J. Phys. (Paris) C 7, 51 (1981); J. Phys. Soc. Jpn. **51**, 2373 (1982).
[4] S. W. Teitsworth, R. M. Westervelt, and E. E. Haller, Phys. Rev. Lett. **51**, 825 (1983).
[5] A. Brandl, W. Kröninger, W. Prettl, and G. Obermair, Phys. Rev. Lett. **64**, 212 (1990).
[6] J. Peinke, J. Parisi, O. E. Roessler, and R. Stoop, *Encounter with Chaos* (Springer, Berlin, 1992).
[7] E. Schöll, in *Handbook on Semiconductors*, 2nd ed., edited by P. T. Landsberg (North-Holland, Amsterdam, 1992), Vol. 1, Chap. 8.

[8]L. V. Keldysh, Zh. Eksp. Teor. Fiz. **37**, 713 (1959) [Sov. Phys. JETP **10**, 509 (1960)].
[9]D. J. Robbins and P. T. Landsberg, J. Phys. C **13**, 2425 (1983).
[10]L. Reggiani and V. Mitin, Nuovo Cimento **12**, 1 (1989).
[11]G. Hüpper, K. Pyragas, and E. Schöll, Phys. Rev. B **47**, 15 515 (1993).
[12]G. Hüpper, K. Pyragas, and E. Schöll, Phys. Rev. B **48**, 17 633 (1993).
[13]T. Kuhn, G. Hüpper, W. Quade, A. Rein, E. Schöll, L. Varani, and L. Reggiani, Phys. Rev. B **48**, 1478 (1993).
[14]E. Schöll and W. Quade, J. Phys. C **20**, L861 (1987).
[15]C. Jacoboni and L. Reggiani, Rev. Mod. Phys. **55**, 645 (1983).
[16]R. Thoma, H. J. Peifer, W. L. Engl, W. Quade, R. Brunetti, and C. Jacoboni, J. Appl. Phys. **69**, 2300 (1991).
[17]L. Varani, L. Reggiani, V. Mitin, C. M. Van Vliet, and T. Kuhn, Phys. Rev. B **48**, 4405 (1993).
[18]M. Lax, Phys. Rev. **119**, 1502 (1960).
[19]V. N. Abakumov, V. I. Perel, and I. N. Yassievich, Fiz. Tekh. Poloprovodn. **12**, 3 (1978) [Sov. Phys. Semicond. **12**, 1 (1978)].
[20]G. Hüpper, Ph.D. thesis, Technical University of Berlin, 1993.
[21]C. Jacoboni and P. Lugli, *The Monte Carlo Method for Semiconductor Device Simulation* (Springer, Wien, 1989).
[22]F. Rossi, P. Poli, and C. Jacoboni, Semicond. Sci. Technol. **7**, 1017 (1992).
[23]K. M. van Vliet and J. R. Fassett, in *Fluctuation Phenomena in Solids,* edited by R. E. Burgess (Academic, New York, 1965), p. 267.
[24]U. Rau, W. Clauss, A. Kittel, M. Lehr, M. Bayerbach, J. Parisi, J. Peinke, and R. P. Hübener, Phys. Rev. B **43**, 2255 (1991).
[25]G. Hüpper and E. Schöll, Phys. Rev. Lett. **66**, 2463 (1991).
[26]W. Clauss, U. Rau, J. Peinke, J. Parisi, A. Kittel, M. Bayerbach, and R. P. Hübener, J. Appl. Phys. **70**, 232 (1991); M. Hirsch, Diploma thesis, University of Tübingen, 1992.
[27]B. Kehrer, W. Quade, and E. Schöll (unpublished).
[28]P. J. van Hall and E. A. E. Zwaal, Superlatt. Microstruct. **13**, 323 (1993).

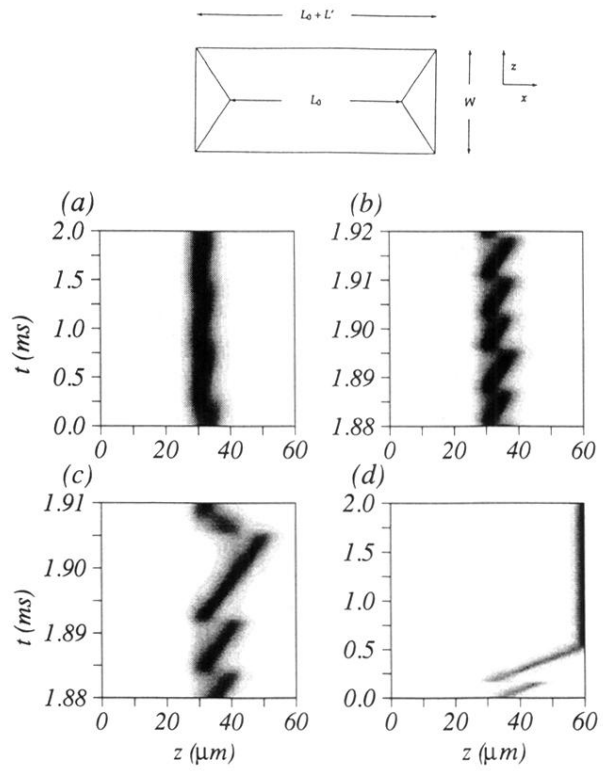

FIG. 10. Density plots of the carrier concentration p as a function of the coordinate z transverse to the electric field, and of time t for different values of the magnetic field. The gray intensity is proportional to the carrier density. (a) $\mathcal{B}=11$ mT, (b) $\mathcal{B}=15$ mT, (c) $\mathcal{B}=20$ mT, and (d) $\mathcal{B}=25$ mT. Numerical parameters as in Fig. 9 with $j_0=0.85$ mA/cm^2. For simplicity a constant mobility $\mu=10^5$ cm^2/V s has been used, which is smaller than in Fig. 2 because of increased N_D. The inset shows the sample configuration with triangular contacts.